Mapping gas exchanges in headwater streams with membrane inlet mass spectrometry

Camille Vautier, Ronan Abherve, Thierry Labasque, Anniet M. Laverman, Aurélie Guillou, Eliot Chatton, Patrick Dupont, Luc Aquilina, Jean-Raynald de Dreuzy

Journal Pre-proofs

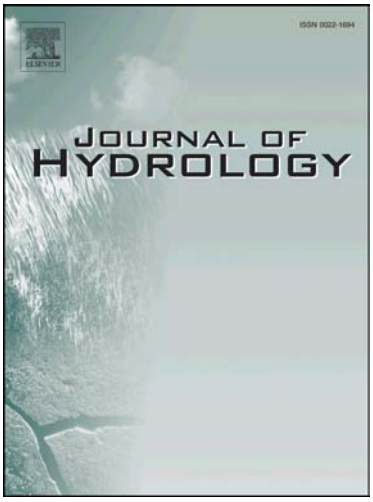

Research papers

Mapping gas exchanges in headwater streams with membrane inlet mass spectrometry

Camille Vautier, Ronan Abhervé, Thierry Labasque, Anniet M. Laverman, Aurélie Guillou, Eliot Chatton, Pascal Dupont, Luc Aquilina, Jean-Raynald de Dreuzy

PII: S0022-1694(19)31133-3
DOI: https://doi.org/10.1016/j.jhydrol.2019.124398
Reference: HYDROL 124398

To appear in: *Journal of Hydrology*

Received Date: 26 July 2019
Revised Date: 20 November 2019
Accepted Date: 22 November 2019

Please cite this article as: Vautier, C., Abhervé, R., Labasque, T., Laverman, A.M., Guillou, A., Chatton, E., Dupont, P., Aquilina, L., de Dreuzy, J-R., Mapping gas exchanges in headwater streams with membrane inlet mass spectrometry, *Journal of Hydrology* (2019), doi: https://doi.org/10.1016/j.jhydrol.2019.124398

Mapping gas exchanges in headwater streams with membrane inlet mass spectrometry

Camille Vautier [a], Ronan Abhervé [a,b], Thierry Labasque [a,c], Anniet M. Laverman [d], Aurélie Guillou [c], Eliot Chatton [a,1], Pascal Dupont [e], Luc Aquilina [a], Jean-Raynald de Dreuzy [a,c]*

[a] Univ Rennes, CNRS, Géosciences Rennes, UMR 6118, 35000 Rennes, France

[b] Centre Eau Terre Environnement, INRS, Quebec City, Canada

[c] Univ Rennes, CNRS, OSUR (Observatoire des sciences de l'univers de Rennes), UMS 3343, 35000 Rennes, France

[d] Univ Rennes, CNRS, Ecobio, UMR 6553, 35000 Rennes, France

[e] LGCGM, INSA Rennes, 35000 Rennes, France

Corresponding Author

* camille.vautier@univ-rennes1.fr

Present Addresses

[1] Sorbonne Universités, UPMC Univ Paris 06, CNRS, Laboratoire d'Océanographie Microbienne (LOMIC), Observatoire Océanologique, Banyuls/mer, France

ABSTRACT

Using continuous injections of helium coupled to *in-situ* continuous flow membrane inlet mass spectrometry (CF-MIMS), we mapped the gas exchanges along two low-slope headwater streams having discharges of 25 L s^{-1} and 90 L s^{-1}. Mean reaeration rate coefficients (k_2) were estimated at 130 d^{-1} and 60 d^{-1}, respectively. Our study revealed that gas exchanges along headwater streams are highly heterogeneous. The variable morphology of the streambed causes gas exchanges to be focused into small areas, namely small cascades made up of stones or wood, with reaeration rate coefficients up to 40 times higher than in low-turbulent zones. As such, cascades appear to be hot spots for both oxygenation and greenhouse gases emissions. Additional O_2 and CO_2 measurements effectively showed fast exchanges between the stream and the atmosphere in the cascades, following the partial pressure gradients. These cascades allow a fast oxygenation of the eutrophic streams depleted in O_2, which sustains respiration. Simultaneously, cascades release the oversaturated CO_2 originating from groundwater inputs to the atmosphere. By comparing measured reaeration rate coefficients to ten predictive equations from literature, we showed that all equations systematically underestimate reaeration rate coefficients, with significantly higher discrepancies in cascades than in low-turbulent zones. The inadequate characterization of the processes occurring in cascades causes empirical

equations to have poor predictive capabilities, leading to a global underestimation of CO_2 emission from headwater streams.

KEY-WORDS

- headwater stream
- membrane inlet mass spectrometry (MIMS)
- reaeration
- gas exchange
- greenhouse gas emission
- CO_2 evasion

HIGHLIGHTS

- *In-situ* membrane inlet mass spectrometry allows real-time mapping of gas exchanges along headwater streams.
- Gas exchange rate coefficients are highly heterogeneous along low-slope headwater streams.
- Predictive equations of gas exchanges are generally reliable in low-turbulent zones, but underestimate gas exchanges in small cascades.
- Small cascades can be viewed as hot spots for both stream oxygenation and CO_2 emission.
- Overlooking small cascades in global CO_2 calculations leads to an underestimation of CO_2 emissions from headwater catchments.

1. INTRODUCTION

Streams continuously exchange gases with the atmosphere. The reaeration process, which characterizes the exchange of oxygen between streams and atmosphere, provides ecosystem services by sustaining in-stream respiration (Aristegi et al. 2009; Knapp et al. 2015). Air-water gas exchanges also control CO_2, CH_4 and N_2O release or uptake by streams (Tranvik et al. 2009) and thus influence the global greenhouse gas budgets of terrestrial systems. Global CO_2 emissions from inland water, estimated at 2.9 PgC y^{-1}, are of the same order of magnitude as terrestrial C sinks of 3.1 PgC y^{-1}. Among inland water CO_2 fluxes, recent studies highlighted the importance of inputs from headwater streams, because of their ubiquity (Bishop et al. 2008), their connection to biologically active compartments and their high level of turbulence (Duvert et al. 2018; Natchimuthu et al. 2017; Öquist et al. 2009; Wallin et al. 2011). Crawford et al. (2014) showed that even in a lake-rich landscape of the Northern Highland Lake District (Michigan, US), streams emitted roughly the same CO_2 mass as lakes. The same study highlighted that streams may also be substantial sources of CH_4 (Crawford et al. 2014). With respect to warming potential, CH_4 emissions by streams corresponded to 26% of the total estimated CO_2 flux. All these studies call for a better quantification of greenhouse gas emissions in lower-order streams.

Quantification of gas exchanges is also crucial in surface water ecology, especially for open-channel metabolism calculations (Aristegi et al. 2009; Knapp et al. 2015). It is a key-point in many hydrogeochemical studies as well, such as radon-based

groundwater discharge estimations (Avery et al. 2018; Cartwright et al. 2014; Cook et al. 2003; Gilfedder et al. 2019; Gleeson et al. 2018). Gas exchange rate coefficients can be measured directly by performing gas tracer release experiments (Benson et al. 2014; Genereux and Hemond 1992; Hall and Madinger 2018; Knapp et al. 2019; Wanninkhof et al. 1990). Inert gases such as propane, SF_6 or helium are injected in the stream, often in conjunction with a non-volatile tracer to account for dispersion and dilution effects. Since these injections are time- and cost-intensive, predictive equations, either empirical (Churchill et al. 1964; Goncalves et al. 2017; Melching and Flores 1999; Tsivoglou and Neal 1976) or process-based (Gualtieri and Gualtieri 2000; Gualtieri et al. 2002), have been developed to propose straightforward estimates of gas exchange rate coefficients. The gas exchange rate coefficients are expressed as a function of hydrodynamic characteristics such as water depth, flow velocity, slope, discharge and in some cases dimensionless numbers (e.g. Froude, Reynolds, Sherwood numbers). A wide diversity of equations may be found in literature, but each equation appears to be specific to the hydrological conditions for which it has been defined, making them poorly reliable at a large scale or in different settings (Melching and Flores 1999; Palumbo and Brown 2014).

The diversity of empirical equations existing in literature reflects the variability of gas exchanges in headwater catchments. Lower-order streams are characterized by the great diversity in small-scale morphological structures, including pools, riffles, and cascades that can change over time and that are difficult to represent at larger

scales. In larger rivers, cascades have been shown to trigger gas exchanges by creating air bubbles (Cirpka et al. 1993). High tracer gas losses have been measured in dams (Caplow et al. 2004). Flume experiments have evidenced that spillways and cascades critically increase water oxygenation (Baylar et al. 2006; Khdhiri et al. 2014; Tebbutt 1972), generating gas exchanges that may be several orders of magnitudes higher than in low-turbulent channels (Baylar et al. 2006). Drops in CO_2 partial pressure downstream from waterfalls have additionally been shown in studies focused on global carbon budget estimates (Wallin et al. 2011) and on river water hardness in karstic systems (Chen et al. 2004). In most studies focused on headwater streams, though, a unique gas exchange rate coefficient is estimated for the whole stream, whatever the diversity of its hydrodynamic conditions.

Here we focus on headwater streams and investigate the impact of small-scale morphological traits on global predictions of gas exchange rate coefficients and CO_2 evasion fluxes. We hypothesize that the heterogeneity of the streambed, which is a characteristic feature of headwater streams, explains the difficulty in predicting gas exchanges and CO_2 emissions. By coupling continuous helium injections and membrane inlet mass spectrometry, we map gas exchanges along two low slope headwater streams that display a diversity of morphological structures. We additionally measure dissolved O_2 and CO_2 to characterize the impact of natural cascades and riffles on stream oxygenation and greenhouse gas emissions in headwater catchments.

2. MATERIAL AND METHODS

The two headwater streams were selected based on the diversity of their morphological structures (i.e. the presence of low-turbulent zones and cascades). Helium (an inert gas tracer) and NaCl (a conservative tracer) were injected continuously and monitored at several distances from the injection site using a continuous flow membrane inlet mass spectrometer (CF-MIMS) and an electrical conductivity (EC) probe. Experiments were performed in spring 2018.

2.1. Study site

The two streams belong to a crystalline catchment located in Pleine-Fougères (Brittany, Western France) (Kolbe et al. 2016). The catchment (figure 1a) is part of the Long-Term Socio-Ecological Research (LTSER) site “Zone Atelier Armorique”. Both streams present typical low-slope headwater stream morphologies, featuring small cascades and low-turbulent areas (figure 1c). Both streams are located in agricultural fields and have riverine vegetation dominated by brambles and diverse herbaceous species such as Kentucky bluegrass and buttercups. Stream A (locally called “Le Ronan”) is a first-order stream with a mean depth of 0.16 m, a mean width of 0.8 m, and a discharge rate of 25 L s^{-1}, as measured by the NaCl slug injection performed the day of the experiment. Stream B (“Le Petit Hermitage”) is a second order stream with a mean depth of 0.25 m, a mean width of 1.8 m, and a discharge rate of 90 L s^{-1}. Their streambeds were covered by heterogeneous detrital elements, such as coarse-grain sediments, small rocks and decaying branches, which led their small-scale morphology to be variable (figure 1b). The global slope of the streams

was deduced from the altitude of the upstream and downstream ends of the reach. The precise topography was then determined by measuring the height of each cascade with a tape. Each reach was divided into several uniform sub-reaches (e.g. low-turbulent zone, cascade). Reach A (total length of 52 m) showed a succession of low-turbulent zones and small cascades (5 to 15 cm high). It was divided into 6 sub-reaches (A_1 to A_6) measuring 3 to 12 meters. Reach B (total length of 98 m) was flat and homogeneous along its first 95 meters, and displayed a 35 cm high cascade at its downstream end, between 95 and 98 meters. It was divided into 3 sub-reaches (B_1 to B_3): two similar segments in the flat zone (B_1 and B_2), and one short segment around the fall (B_3) (figure 1b).

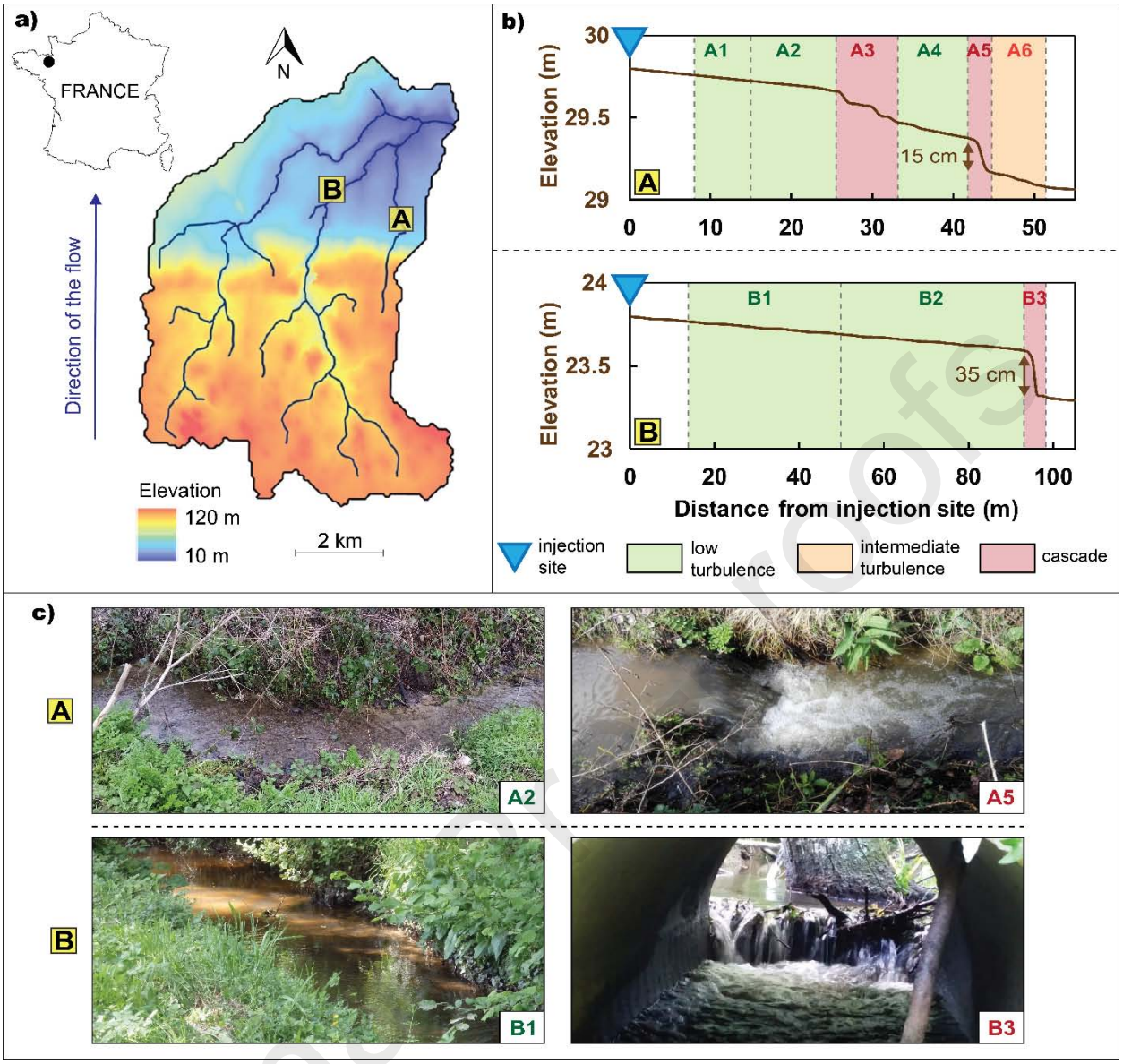

Figure 1. (a) Localization and map of the Pleine-Fougères catchment**, (b)** Streambed topographic profiles of reaches A and B, and **(c)** Pictures of the less turbulent zone (left) and of the highest cascade (right) in reach A (up) and in reach B (down). On the topographic profiles (b), dashed lines indicate sub-reaches limits, colors indicate visually-determined turbulence levels of each sub-reach.

2.2. Tracer injection

Helium was chosen as gaseous tracer for the following reasons. (1) As a noble gas, it is non-reactive. (2) It is non-toxic. (3) Its concentration in the atmosphere is very low (around 5 ppm), allowing a high concentration difference between stream and atmosphere during injections. (4) It can be accurately measured with CF-MIMS and gas chromatography. (5) It is highly volatile, increasing the accuracy of degassing estimations. (6) It is not expensive. (7) Unlike other tracers such as SF_6 (Benson et al. 2014), it is not a greenhouse gas. A non-volatile conservative tracer was also needed to account for potential dilution due to groundwater discharge (Genereux and Hemond 1990; Kilpatrick et al. 1987; Tobias et al. 2009). We used chloride from NaCl, which is classically chosen for its low cost and simple use (Genereux and Hemond 1990; Genereux and Hemond 1992).

Helium and NaCl were injected continuously at a constant rate for 2 hours in stream A and for 1 hour in stream B. Helium was injected from a 100% liquid helium bottle through bubbling on the stream bottom (Supplementary data, Figure A.1). A precision manometer and a pressure regulator ensured the stability of the injection. The background helium concentration of both streams was around 8.10^{-9} mol L^{-1}. Upon injection, it increased to 1.10^{-7} mol L^{-1} in stream A and to 8.10^{-7} mol L^{-1} in stream B. 10 kg of NaCl were dissolved in a 300 L can filled with stream water. The NaCl solution was then injected into the stream at a flow rate of 2 L min^{-1} using a peristaltic pump. The background electrical conductivity, measured at the injection site, before and after the experiments, was 270 µS cm^{-1} in

stream A and 204 µS cm^{-1} in stream B. Upon injection, it increased to 330 µS cm^{-1} in stream A and to 229 µS cm^{-1} in stream B.

2.3. Measurement

In-situ measurements of helium were performed using continuous flow membrane inlet mass spectrometry (CF-MIMS). *In-situ* membrane inlet mass spectrometry has been shown to improve the determination of gas exchange rate coefficients based on tracer injections (Knapp et al. 2019). It was also used recently by Weber et al. (2019) to derive gas exchange rate coefficients from direct measurements of dissolved atmospheric gases. The CF-MIMS used here (modified from HPR40 - Hiden Analytical) is described in details in Chatton et al. (2017). The gas inlet is ensured by a membrane (X44® 99) connected to the vacuum of a Quadrupole Mass Spectrometer (QMS around 10^{-5} Torr), allowing the direct permeation of dissolved gases from water to spectrometer. Inside the QMS, gases are ionized using an oxide coated iridium filament that allows the selection of ionization energies (between 4 and 150 eV) and emission intensities (between 20 and 5000 µA). Ionized gases are then separated by the quadrupole according to their mass to charge ratios. Then, the detection of gases is performed either by a Faraday cup or a single channel electron multiplier (SCEM). The instrumental relative standard deviation is 2% for He and 0.2% for N_2, O_2 and CO_2, indicating high measurement sensitivity.

The spectrometer was installed a few meters away from the stream. Stream water was pumped continuously (MP1 Grunfoss pump, 5 L min^{-1}) and brought to the spectrometer membrane through a nylon tubing system preventing any contact with

the air. The pump was attached to a float so that stream water was pumped at a constant depth, approximately 10 cm below the surface. Helium was measured by the spectrometer in real time, with a 10 second timestep. During injection, the pump feeding the CF-MIMS was moved step by step from the downstream end to the upstream end of the reach to map the loss of helium along the stream. To make sure that the injection rate was constant, the pump was first installed at the downstream end of the reach until helium concentrations reached a stable plateau for 20 minutes. Then, the pump was moved a few meters upstream to the next measurement location. After a few minutes of unstable measurements due to pump and tubing manipulation, the helium concentration stabilized at a new stable plateau. From that time, the pump was maintained at this location during 10 minutes to gather a significant number of helium measurements (60 to 70) and make sure the injection rate was constant. Then the pump was moved upstream to the next measurement location, and the procedure was reiterated up to the uppermost measurement location. Moving the pump upstream avoided perturbation from one measurement location to the next one. The stability of the injection and the consistency of the measurements were checked continuously using real-time data visualization provided by the *in-situ* CF-MIMS system. This system allowed real-time mapping of the degassing taking place along the streams. Major atmospheric gas concentrations (N_2, O_2, Ar, CO_2), water vapor pressure (H_2O) and temperature were simultaneously measured with the CF-MIMS to correct helium data for external and instrumental deviations. CF-MIMS data, expressed in partial pressures in air, were converted into concentrations in water by

external calibration with micro-gas chromatography (µGC) measurements on grab samples. Two samples intended for µGC analysis were taken at each location, in 500 mL glass bottles. To ensure the synchronicity of CF-MIMS and µGC data, samples were collected directly at the CF-MIMS outlet. The tube filling the glass bottles was immerged in a bucket to avoid any contact with the atmosphere. All µGC measurements were performed less than 48 hours after sampling. The instrument relative standard deviation of the µGC is 3%. Detailed description of CF-MIMS measurements, corrections and the calibration procedure can be found in Chatton et al. (2017). As a proxy for NaCl, electrical conductivity was monitored using two Hatch® probes. The relative standard deviation of EC measurements is 5%. One EC probe was moved together with the pump. The probe and the pump were attached to the same float to ensure they sampled the same water. The second EC probe was permanently installed 10 meters downstream from the injection site to check the stability of salt injection. The experimental set-up is summarized in figure 2.

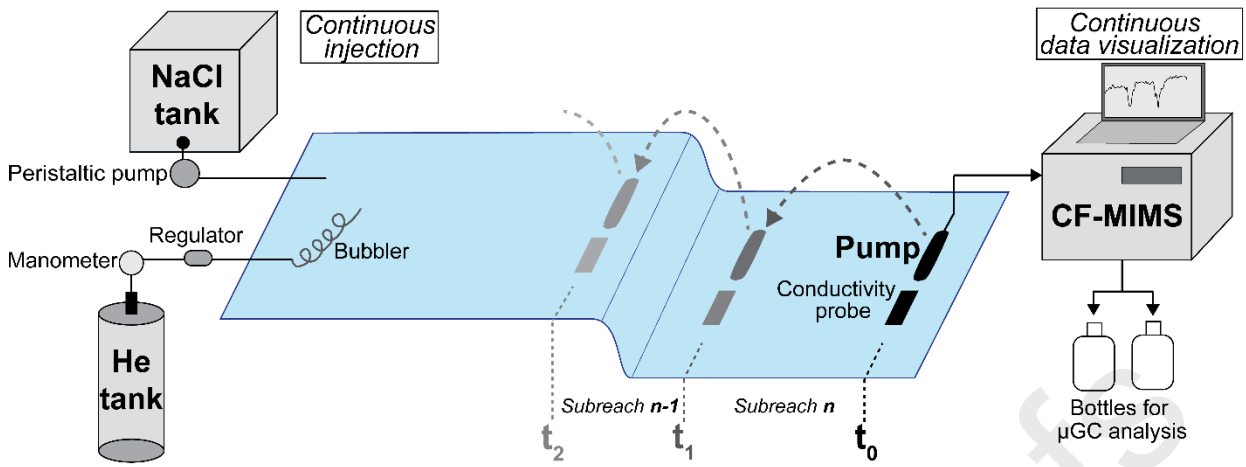

Figure 2. Experimental set up. Upstream, helium and salt are injected continuously at a stable level during the whole duration of the experiment. Downstream, at decreasing distances from the injection site, helium concentrations are measured continuously and visualized in real-time using a CF-MIMS fed by a pump. Chloride concentrations are measured with an EC probe. First, the pump and the EC probe are installed at the downstream end of the reach (t_0). Once the concentration in helium reaches a plateau, the pump and the EC probe are moved upstream to the next measurement location (t_1). Once a new plateau in concentration is reached, instruments are moved upstream again (t_2). The procedure is reiterated up until the last measurement location to map helium losses along the whole length of the reach. In order to calibrate CF-MIMS measurements, two bottles are sampled from the CF-MIMS outlet at each measurement location for µGC analysis.

2.4. Calculation of gas exchange rate coefficient

Degassing is commonly assumed to be linearly proportional to the air-water concentration difference (Kilpatrick et al. 1987). Thus, the variation in helium concentrations through time can be expressed by the 1D advection-dispersion equation:

$$\frac{\partial C_{He}}{\partial t} + U\frac{\partial C_{He}}{\partial x} = D_x\frac{\partial^2 C_{He}}{\partial x^2} - k_{He}(C_{He} - C_{He}^{eq}) \quad (1)$$

where C_{He} (mol L^{-1}) is the helium concentration, C_{He}^{eq} (mol L^{-1}) is the helium concentration in a stream at equilibrium with the atmosphere, k_{He} (s^{-1}) is the air-water gas exchange rate coefficient of helium, U (m s^{-1}) is the water velocity and D_x (m^2 s^{-1}) is the longitudinal dispersion coefficient. Since helium has a low atmospheric concentration, its equilibrium concentration in stream is low (around 8.10^{-9} mol L^{-1}). Thus, during helium injections, stream helium concentration becomes at least one order of magnitude higher than the equilibrium concentration, and C_{He}^{eq} can be neglected. The variations in chloride concentrations through time can be expressed using the same advection-dispersion equation without the degassing term:

$$\frac{\partial C_{Cl}}{\partial t} + U\frac{\partial C_{Cl}}{\partial x} = D_x\frac{\partial^2 C_{Cl}}{\partial x^2} \quad (2)$$

where C_{Cl} (mol L^{-1}) is the chloride concentration. Assuming that the advection and dispersion parameters for chloride are similar than for helium (Genereux and Hemond 1992; Tobias et al. 2009; Wanninkhof et al. 1990), combining equations 1

and 2 leads to the solution proposed by Kilpatrick et al. (1987), in which dilution effects are taken into account by the ratio in chloride concentrations:

$$k_{He} = \frac{U}{L} ln \left(\frac{\frac{C_{He}^{up}}{C_{He}^{down}}}{\frac{C_{Cl}^{up}}{C_{Cl}^{down}}} \right) \quad (3)$$

where C_{He}^{up} and C_{Cl}^{up} (mol L^{-1}) are the upstream concentrations, C_{He}^{down} and C_{Cl}^{down} (mol L^{-1}) are the downstream concentrations, U (m s^{-1}) is the mean stream velocity and L (m) is the distance between the two locations.

The gas exchanges depend on the nature of the gas and on water temperature. Gas exchange rate coefficients can be scaled from one gas to another using the ratio of their Schmidt numbers (Jähne et al. 1987b). The Schmidt number (Sc) is a dimensionless number corresponding to the ratio of kinematic viscosity to mass diffusivity. To enable comparison with previously published results, gas exchange rate coefficients calculated for helium, k_{He}, are scaled to the reaeration rate coefficient k_2, defined as the gas exchange rate coefficient for O_2 at 20°C:

$$k_2 = k_{He} \left(\frac{Sc_{O_2}}{Sc_{He}} \right)^{-0,5} \quad (4)$$

where Sc_{O2} is the Schmidt number for oxygen at 20°C and Sc_{He} is the Schmidt number for helium at stream temperature. The equations from which the Schmidt numbers used in this study were obtained are featured in table 1.

Table 1. Schmidt numbers used in this study.

Gas	Reference	Equation
He	Wanninkhof (1992) based on data from Jähne et al. (1987a)	$Sc_{He} = 377.09 - 19.154\ T + 0.50137\ T^2 - 0.005669\ T^3$
O_2	Baird and Davidson (1962); Carlson (1911); Raymond et al. (2012); Wise and Houghton (1966)	$Sc_{O_2} = 1568 - 86.04\ T + 2.142\ T^2 - 0.0216\ T^3$
CO_2	Wanninkhof (1992)	$Sc_{CO_2} = 1911 - 118.11\ T + 3.453\ T^2 - 0.0413\ T^3$

2.5. Comparison with predictive equations

Gualtieri et al. (2002) performed a dimensional analysis to identify the physical parameters that control gas exchange rate coefficients in streams. They showed that gas exchange rate coefficients k (d^{-1}) can be expressed as a direct function of the Froude number Fr, the channel slope i, the Reynolds number Re, the ratio between the stream depth h (m), the mean velocity U ($m\ s^{-1}$), and a dimensionless gas exchange factor λ:

$$k = \frac{U}{h}\lambda[Fr,i,Re] \tag{5}$$

with: $$Fr = \frac{U}{\sqrt{gh}} \quad ; \quad Re = \frac{U\,h}{\nu}$$

where g (m s^{-2}) is the gravitational acceleration and ν (m^2 s^{-1}) is the kinematic viscosity. Gualtieri et al. (2002) reformulated 20 empirical and semi-empirical equations from literature as a function of these parameters. It was shown that all equations physically contain the velocity over depth ratio, the slope and the Froude number. Some of them additionally involve the Reynolds number. Their process-based analysis pointed out that stream depth is a crucial parameter in any gas exchange rate coefficient equation: it influences in the velocity over depth ratio as well as the Froude and Reynolds numbers. Thus, application of these equations implicitly assumes the existence of a water layer with a well-defined thickness. In cascades, such a layer cannot be defined. A cascade can be seen as a succession of a ramp, where gas exchanges occur at the free surface of the water layer, and a receiving basin, in which gas exchanges are controlled by air bubbles (Cirpka et al. 1993). In the ramp section of the cascade, the supercritical flow regime implies that the water layer is very thin and uneven. In the receiving basin portion of the cascade, the falling jet penetrating the water generates high turbulence and uneven flows. Thus, the empirical and semi-empirical equations of gas exchange rate coefficient are theoretically not applicable in cascades. Cirpka et al. (1993) developed alternative semi-empirical equations to describe gas exchanges specifically within cascades in large rivers. Their equations account for gas exchanges through the free surface and via air bubbles. They rely on four parameters, the calibration of which

requires extensive in-situ tracer experiments with the simultaneous injections of four different gases.

This raises the question of the suitability of predictive equations for global estimations of gas exchange rate coefficients. Indeed, since most headwater streams display both cascades and low turbulent zones, the unreliability of equations in cascades is likely to distort the gas exchange rate coefficient at the stream scale. To test if the presence of a few cascades significantly distorts global gas exchange predictions over a stream reach, we compared measured k_2 values with values calculated using predictive equations developed for small streams (table 2). We considered the historical equation of O'Connor and Dobbins (1958). Among the many other empirical equations that have been proposed ever since, we chose the relationships that were calibrated with the largest datasets. The semi-empirical equation from Melching and Flores (1999) is based on a large USGS data set and was further used in several studies (Haider et al. 2013; Ritz et al. 2017). The seven semi-empirical equations from Raymond et al. (2012) are based on the same USGS data set and on four additional data sets (Bernot et al. 2010; Bott et al. 2006; Mulholland et al. 2001; Tsivoglou and Neal 1976), making them, to our knowledge, the equations based on the largest amount of data (Lauerwald et al. 2015). We also considered the process-based equation proposed by Gualtieri and Gualtieri (2000) and Gualtieri et al. (2002).

Table 2. Predictive equations considered in this study. All formulas were converted into the reaeration rate coefficient k_2 (d^{-1}).

Reference	Equation type		Equation
O'Connor and Dobbins (1958)	Semi-empirical		$k_2 = 3.93\ U^{0.5}\ h^{-1.5}$
Melching and Flores (1999)	Semi-empirical		$k_2 = 517\ (Ui)^{0.524}\ Q^{-0.242}$
Gualtieri and Gualtieri (2000) Gualtieri et al. (2002)	Process-based		$k_2 = 86400\ \frac{U}{h}\ \frac{2^{1/3}}{Sc^{2/3}\ {R_{m-t}}^{2/3}}\ Re^{-1/3}\ Fr^{-2/3}\ i^{1/3}$
Raymond et al. (2012)	Semi-empirical	[1]	$k_2 = 5354\ (Ui)^{0.89}\ h^{-0.46}$
		[2]	$k_2 = 6311\ (Ui)^{0.89}\ h^{-0.42}\ (1 - 2.54\ Fr^2)$
		[3]	$k_2 = 1235\ U^{0.85} s^{0.77}\ h^{-1}$
		[4]	$k_2 = 1011\ (Ui)^{0.76}\ h^{-1}$
		[5]	$k_2 = (3020\ Ui + 2.15)\ h^{-1}$
		[6]	$k_2 = 988\ (Ui)^{0.75}\ Q^{0.011}\ h^{-1}$
		[7]	$k_2 = 5023\ (Ui)^{0.86}\ Q^{-0.14}\ h^{-0.34}$

To compare measured gas exchange rate coefficients with gas exchange rate coefficients obtained using predictive equations, the hydraulic parameters of each stream were measured. (Supplementary data, Table A.1). Global parameters were

evaluated at the reach scale and local parameters were evaluated for each sub-reach. Stream discharge was calculated using a NaCl slug injection. Velocity was measured using a field velocimeter (FP111 Global Water Flow Probe). The slope was derived from the altitude gradient between upper and lower reach ends. Depth was measured at several points across and along each reach, and averaged for each reach.

2.6. Reactive gases

In conjunction with helium, O_2 and CO_2 were measured by CF-MIMS at several distances from the injection site. Measurements were externally calibrated using micro-gas chromatograph (µGC) measurements, in the same way as for helium. In both streams, the helium enrichment due to the injection was less than 1 µmol L^{-1}, so it did not induce significant degassing of O_2 or CO_2. In stream B, O_2 and CO_2 measurements failed because of a calibration error of the µGC.

CO_2 evasion was calculated using the measured CO_2 concentrations and the gas exchange rate coefficient derived from the helium injection. Gas exchange rate coefficients were first converted from He to CO_2 based on the ratio of their Schmidt numbers (equation 4). The Schmidt number for CO_2 is given in table 1. The CO_2 evasion rate at the stream-atmosphere interface (mol m^{-2} s^{-1}) was then calculated using the flux equation first developed for reaeration by Young and Huryn (1998) and later derived for CO_2 evasion (Billett et al. 2004; Hope et al. 2001; Öquist et al. 2009; Wallin et al. 2011) :

$$CO_{2\,evasion} = (CO_{2\,stream} - CO_{2\,eq}) \times k_{CO_2} \times \frac{Q}{U \times w} \qquad (6)$$

where $CO_{2\ stream}$ is the measured CO_2 concentration (mol L^{-1}), $CO_{2\ eq}$ is the concentration at equilibrium with the atmosphere (mol L^{-1}), k_{CO2} is the gas exchange rate coefficient for CO_2 (s^{-1}), Q is the stream discharge (L s^{-1}), U is the mean velocity of the water (m s^{-1}) and w is the stream width (m).

2.7. List of the parameters

The parameters used in the paper are listed in table 3.

Table 3. List of parameters used in the paper.

Symbol	Variable	Unit
C_{Cl}	concentration of chloride	mol L^{-1}
C_{Cl}^{down}	downstream concentration of chloride	mol L^{-1}
C_{Cl}^{up}	upstream concentration of chloride	mol L^{-1}
C_{He}	concentration of helium	mol L^{-1}
C_{He}^{eq}	concentration of helium at equilibrium with the atmosphere	mol L^{-1}
C_{He}^{down}	downstream concentration of helium	mol L^{-1}
C_{He}^{up}	upstream concentration of helium	mol L^{-1}
D_x	longitudinal dispersion coefficient	m^2 s^{-1}
E	Aeration efficiency	[]
Fr	Froude number	[]
g	standard acceleration due to gravity	m s^{-2}
h	water depth	m
i	slope	[]
k	gas exchange rate coefficient	s^{-1}
k_2	gas exchange rate coefficient for O_2 at 20°C *(also called reaeration rate coefficient)*	s^{-1}

k_{He}	gas exchange rate coefficient for He at the stream temperature	s^{-1}
L	stream length	m
Q	stream discharge	$m^3\ s^{-1}$
Re	Reynolds number	[]
$R_{m\text{-}t}$	mass transfer Reynolds number (fitted with data)	[]
Sc_{CO2}	Schmidt number for CO_2	[]
Sc_{He}	Schmidt number for He	[]
Sc_{O2}	Schmidt number for O_2	[]
T	stream temperature	°C
t	time	s
U	Stream velocity	$m\ s^{-1}$
x	Distance	m
w	Stream width	m
λ	Dimensionless gas exchange factor	[]
ν	kinematic viscosity	$m^2\ s^{-1}$

3. RESULTS

3.1. Gas exchange mapping

In both streams (A and B), measurements at several distances from the injection site show a decrease in helium concentrations from upstream to downstream (figure 3). In stream A, the helium concentrations decrease from 140 nmol L^{-1} at 14 m from the injection site to 84 nmol L^{-1} at 52 m downstream. A light rain event occurred at the end of the experiment, just before the pump was set up at the most upstream measurement location (9 m). The rain increased the gas exchanges at the stream surface (Ho et al. 2000), leading to lower helium concentrations at 9 m (130

nmol L^{-1}) than at 14 m (140 nmol L^{-1}). In stream B, helium concentrations decrease from 820 nmol L^{-1} at 15 m from the injection site to 650 nmol L^{-1} at 98 m downstream. The CF-MIMS semi-continuous measurements allowed visualization and quantification of the uncertainty in helium concentration estimates. The relative standard deviation (RSD) of the 60 to 70 measurements available at each distance was comprised between 1.7 and 4.5% in stream A, and between 0.9 and 1.5% in stream B, attesting the stability of helium concentrations at each location. The lower RSD in stream B is probably due to the higher helium injection rate. The large number of measurements allows to perform a trend analysis on each plateau. It reveals the absence of systematic decrease or increase of the helium concentration upon a plateau (Supplementary data, Table A.2). In stream A, 4 plateaus have a slight increasing trend and 3 plateaus have a slight decreasing trend. In stream B, 3 plateaus have a slight increasing trend and one plateau has a slight decreasing trend. This suggest an overall stability of the injection rate. Electrical conductivity can be considered as stable along the streams, since its variation from upstream to downstream is lower than the instrumental relative standard deviation. EC stability thus shows the absence of major groundwater inputs prone to modify the helium signal. In stream A, where measurements of O_2 and CO_2 are available, the consistency in the variations of He, O_2 and CO_2 further confirms the absence of disturbance of the gas content by groundwater inputs. CO_2 concentrations in groundwater, as measured at a small spring located 20 meters upstream from the injection site, reach 650 µmol L^{-1}, that is 30 times the atmospheric equilibrium.

Inputs of such concentrated groundwater along the studied reach would have induced a sharp increase in CO_2 concentrations in the stream. However, CO_2 concentrations follow a general decreasing trend, from at 299 µmol L^{-1} at 14 m to 288 µmol L^{-1} at 52 m, suggesting that there are no major inputs of groundwater along the studied reach. Salt injections had to be stopped before the end of the experiments because of a deficit in salt injection solution. It is unlikely to bias the conclusions reached here, as EC does not change between the downstream and upstream ends of each studied reach (figure 3).

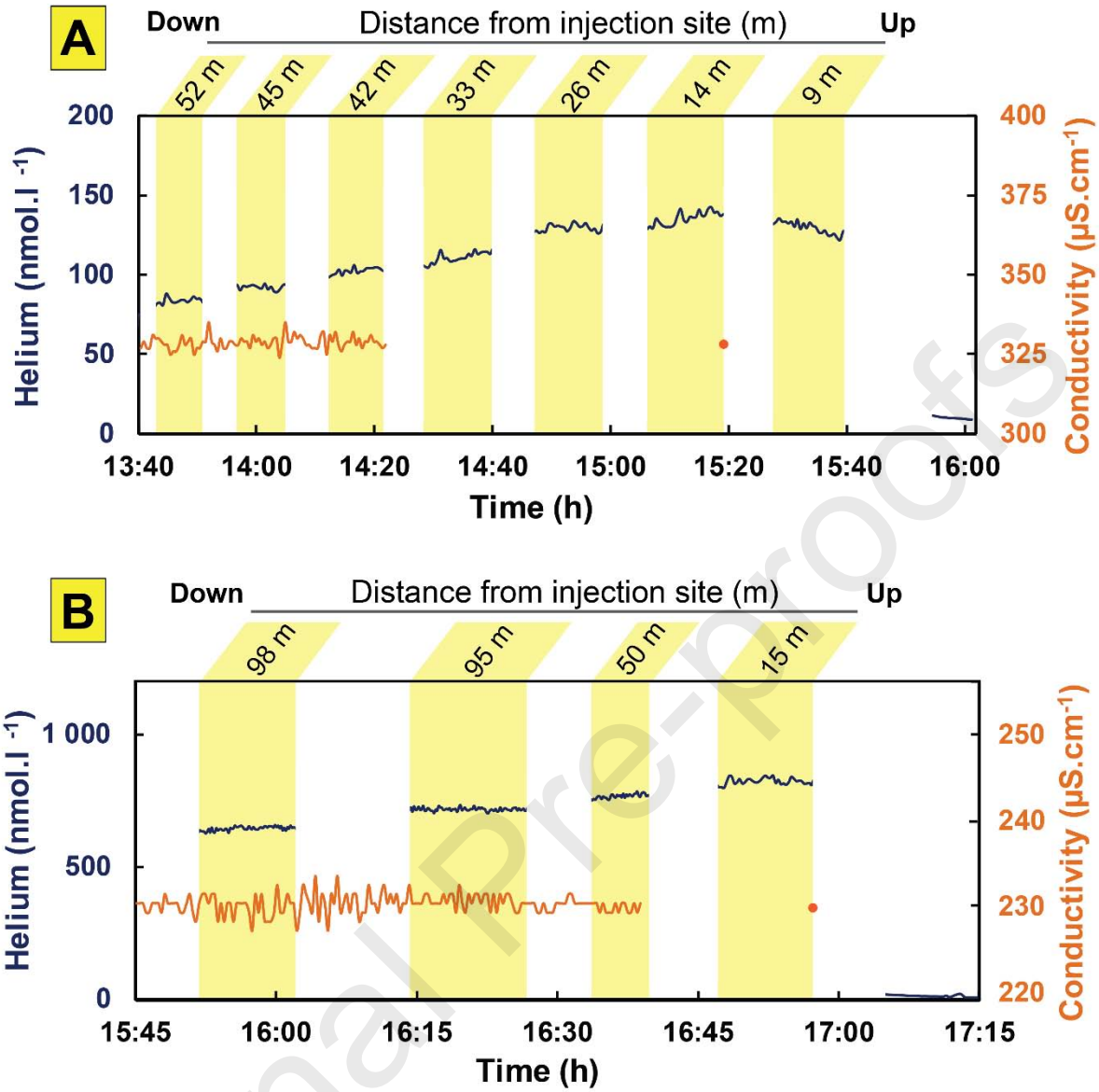

Figure 3. Monitoring of helium in stream A (up) and B (down). Blue lines represent the calibrated helium concentration, orange lines represent the electrical conductivity. Each plateau, highlighted by a yellow band, corresponds to a measurement location. Salt injection was stopped at 14:20 in stream A and at 16:40 in stream B. In stream A, it rained at the end of the experiment, when the pump was at 9 m from the injection site. Rain increased gas exchanges between stream and atmosphere thus lowering helium concentrations. The complete helium time series, including the measurements during the changes of measurement location, are presented in the Supplementary data, Figure A.2.

Global gas exchange rate coefficients in each stream were calculated using the concentration difference between the most upstream and downstream locations (equation 3). Since EC does not vary along each stream, the ratio between upstream and downstream chloride concentrations is equal to 1 and can be simplified in equation 3. The gas exchange rate coefficient for helium, k_{He}, was 196 d^{-1} in stream A and 99 d^{-1} in stream B, corresponding to a reaeration rate coefficient, k_2, of respectively 130 d^{-1} and 60 d^{-1} (equation 4). These k_2 are in the range of values found by other gas tracer release experiments in headwater streams (table 4). The reaeration rate coefficient is significantly higher in the 1st order stream (A) than in the 2nd order stream (B). It is consistent with the observations of Wallin et al. (2011) showing an increase in the rate of CO_2 degassing with lower stream order.

Table 4. Reaeration rate coefficients measured in this study are in the range of reaeration rate coefficients from other gas tracer release experiments performed in headwater streams (Q < 100 L s^{-1}).

Reference	Gaseous tracer	Non-volatile tracer	k_2 (d^{-1})
This study, stream A	**He**	**chloride**	**130**
This study, stream B	**He**	**chloride**	**60**
Wanninkhof et al. (1990)	SF_6	^3H_2O	119
Genereux and Hemond (1992)	propane, ethane	chloride	118 – 139
Soares et al. (2013)	propane	rhodamine WT	27 – 367
Benson et al. (2014)	SF_6, Xe	-	47 – 66
Knapp et al. (2019)	propane, krypton	fluorescein	15 – 134

For each sub-reach, reaeration rate coefficients were calculated in the same way as for the full stream reaches. Helium concentrations and reaeration rate coefficients were then reported as a function of the distance from injection site (figure 4). Uncertainties in the helium concentrations were estimated by the standard deviations of the 60 to 70 CF-MIMS measurements available for each plateau. Standard deviations are small (figure 4), demonstrating the robustness of the measurements. Uncertainties in the gas exchange rate coefficients were estimated by randomly subsampling each plateau of helium concentration. The gas exchange rate coefficient was calculated using a randomly chosen value of the upstream plateau and a

randomly chosen value of the downstream plateau. The random sampling was reiterated 1000 times for each sub-reach, leading to 1000 k_2 values. The standard deviation of the 1000 k_2 values indicated the uncertainty due to helium measurement (figure 4). The uncertainty is smaller in stream B than in stream A, due to the lower noise level in stream B. A big advantage of the continuous measurements with in-situ CF-MIMS is that it produces a significant number of measurements, which allows to visualize and quantify the uncertainties. For the sub-reaches where EC was available, the uncertainty due to EC measurements was quantified in the same way, by sub-sampling EC values from each plateau. Taking into account the uncertainty due to EC measurements increased the standard deviation by 50% in sub-reach A_5, by 8% in sub-reach A_6 and by 10% in sub-reach B_3. Thus, the uncertainty due to EC measurements is lower than the uncertainty due to helium measurements, but is not negligible. When possible, we recommend using a fluorescent dye as conservative tracer, rather than NaCl. The measurement accuracy of fluorescent dyes is usually higher, and florescent dyes are not present naturally in water, which lowers the overall uncertainty on gas exchange rate coefficients.

The gas exchanges are heterogeneously distributed along the streams. In stream A, k_2 increases by a factor of 6 from the less turbulent zones ($k_2(A_2) = 50$ d^{-1}; $k_2(A_4) = 70$ d^{-1}) to the highest cascade ($k_2(A_5) = 360$ d^{-1}). Intermediary values are found in the sub-reach displaying three successive small cascades ($k_2(A_3) = 220$ d^{-1}) and in the agitated sub-reach with no identifiable cascade ($k_2(A_6) = 140$ d^{-1}). Thus, reaeration rate coefficients are ranked according to the level of turbulence. In stream

B, the range of reaeration rate coefficients is larger. The reaeration rate coefficient is 40 times higher in the cascade ($k_2(B_3) = 1030\ d^{-1}$) than in the flat area ($k_2(B_1) = k_2(B_2) = 25\ d^{-1}$). Note that the first two sub-reaches B_1 and B_2, presenting visually the same morphological characteristics, have the same k_2 values, which supports the reliability of the method. This mapping of gas exchanges evidences a high heterogeneity of degassing along the streams. Exchanges are strongly focused in cascades: a 35 cm high cascade loses as much gas as an 80 m long low-turbulent reach.

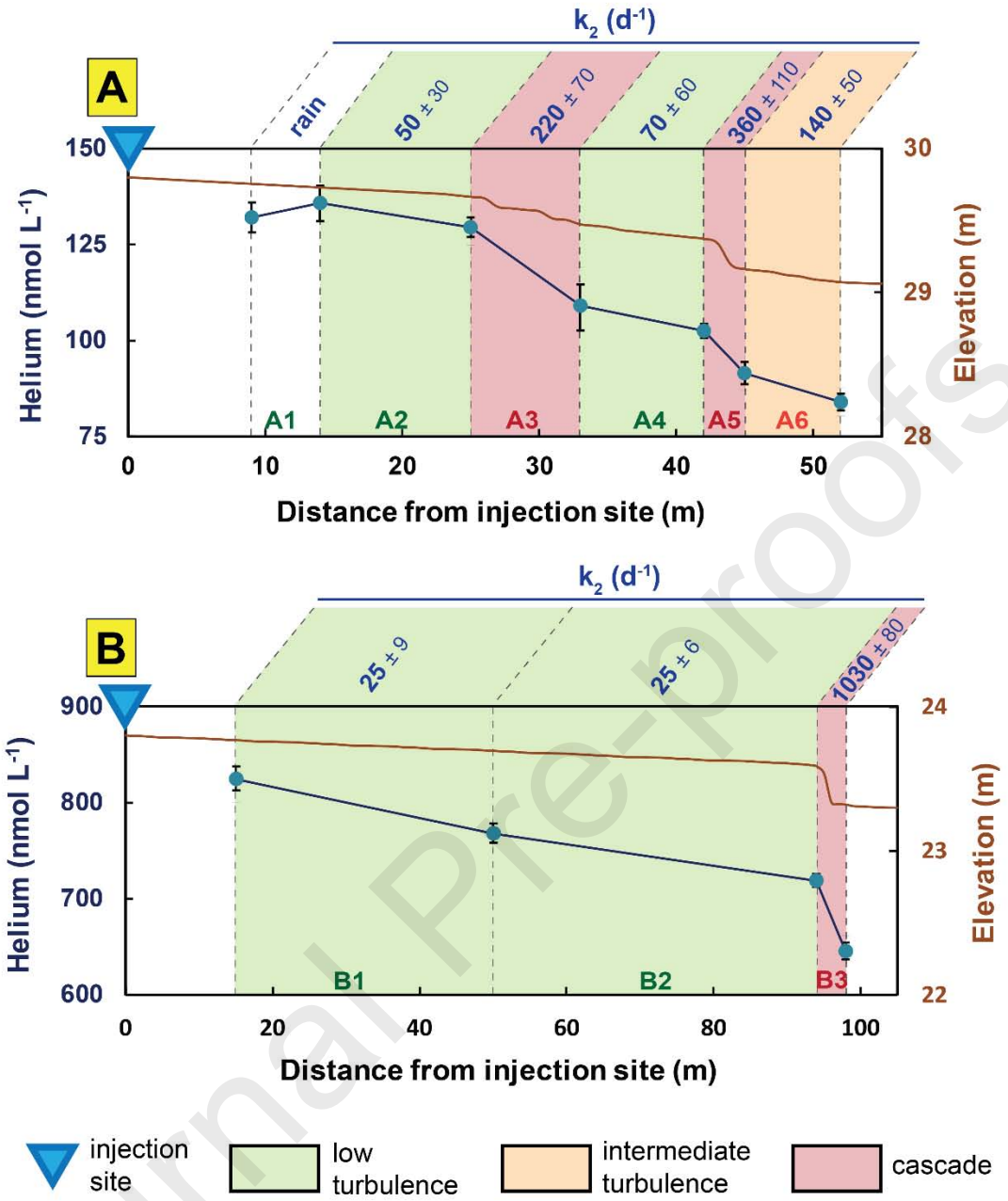

Figure 4. Helium loss along stream A (top) and stream B (bottom) as a function of the distance from the injection site. Helium concentrations were calculated at each location as the average of the plateau highlighted in figure 3. In stream A, it rained at the end of the injection, inducing higher gas exchanges between stream and atmosphere that lowered helium concentrations measured at 9 m from injection site. Error bars in the helium concentration represent ± σ. On top of each graph, reaeration rate coefficients are given (k_2). The confidence intervals of the reaeration rate coefficient, determined by a subsampling of each plateau of helium concentration, represent ± σ.

3.2. Suitability of predictive equations

The ten predictive equations given in table 2 were applied to the streams A and B using the hydraulic parameters given in table A.1. At the reach scale, the ten predictive equations systematically underestimate reaeration rate coefficients, by a factor comprised between 1.2 and 2.2 (figure 5). Reaeration rate coefficients were also calculated for each sub-reach using the local hydraulic parameters. The mean and standard deviation of the ten predicted k_2 values (obtained with the ten equations of table 2) are given in table 5. On average, predictive equations strongly underestimate gas exchanges in the cascade sub-reaches, while they are consistent in low-turbulent zones. The spread of the k_2 values given by the different equations, indicated by their standard deviation, is also significantly higher in cascades than in low-turbulent zones. Elevated differences between predicted and measured k_2 values

in cascades are due to the fact that physically, predictive equations are non-reliable in high-turbulent zones (section 2.5). They are based on parameters that are highly difficult to measure in cascades such as the stream depth. The underestimation of predicted reaeration rate coefficients in cascades significantly biases the predictions at the full-reach scale, leading to a systematic underestimation of global gas exchanges.

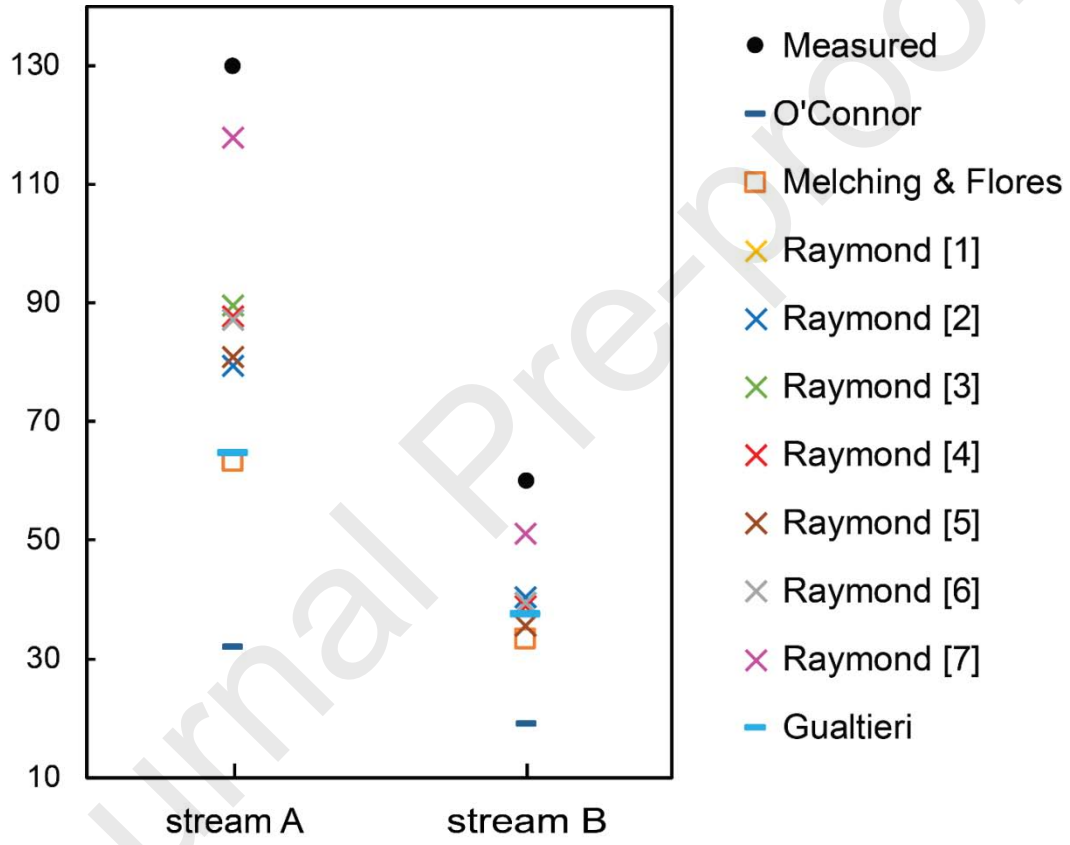

Figure 5. Predictive equations systematically underestimate the reaeration rate coefficient measured at the full-reach scale.

Table 5. Comparison of predicted and measured reaeration rate coefficients in each sub-reach. The mean and standard deviation of the predicted k_2 derive from the statistics of the values obtained with the ten equations of table 2.

Stream	Sub-reach	Agitation level	Measured k_2 (d^{-1})	Mean of the predicted k_2 (d^{-1})	Standard deviation of the predicted k_2 (d^{-1})
A	A2	calm	50	47	8
	A3	**cascade**	**220**	**111**	**38**
	A4	calm	70	61	13
	A5	**cascade**	**360**	**189**	**81**
	A6	intermediate	140	86	26
B	B1	calm	25	22	3
	B2	calm	25	22	3
	B3	**cascade**	**1030**	**679**	**441**

3.3. Impacts on reactive gases

With a mean concentration of around 290 µmol L^{-1}, stream A is oversaturated in CO_2, in the sense that it contains 10 times more CO_2 than it would at equilibrium with the atmosphere (figure 6). CO_2 oversaturation is frequent in headwater streams, because of inputs of groundwater that are highly concentrated in CO_2 due to the aerobic degradation of organic matter (Cole et al. 2007). Water-rock interaction can also be a source of CO_2 in streams, especially in karst regions (Chen et al. 2004). The large excess of CO_2 in stream A originates from a small spring that flows 20 meters upstream from the injection site. The spring water has a CO_2 concentration

reaching 650 µmol L^{-1}, which is 30 times higher than the atmospheric equilibrium. Contrariwise, stream A shows an undersaturation in O_2 (figure 6). Its O_2 concentration is comprised between 280 and 300 µmol L^{-1}, while at equilibrium with the atmosphere it would be 344 µmol L^{-1}. Undersaturation in O_2 is common in headwater streams because they are mostly net heterotrophs (Knapp et al. 2015; Riley and Dodds 2012; Young and Huryn 1999). In cascades, the state of the stream is rapidly modified by strong exchanges of gas following partial pressure gradients. CO_2 oversaturation induces significant drops in CO_2 in cascades, while O_2 undersaturation induces gains in O_2 (figure 6). Release of CO_2 to the atmosphere, as well as stream oxygenation, mainly occurs in the cascades. Note that the rain event that occurred when the pump was at 9 m from the injection site increased gas

exchanges, leading to a drop in CO_2 concentration and an increase in O_2 concentration.

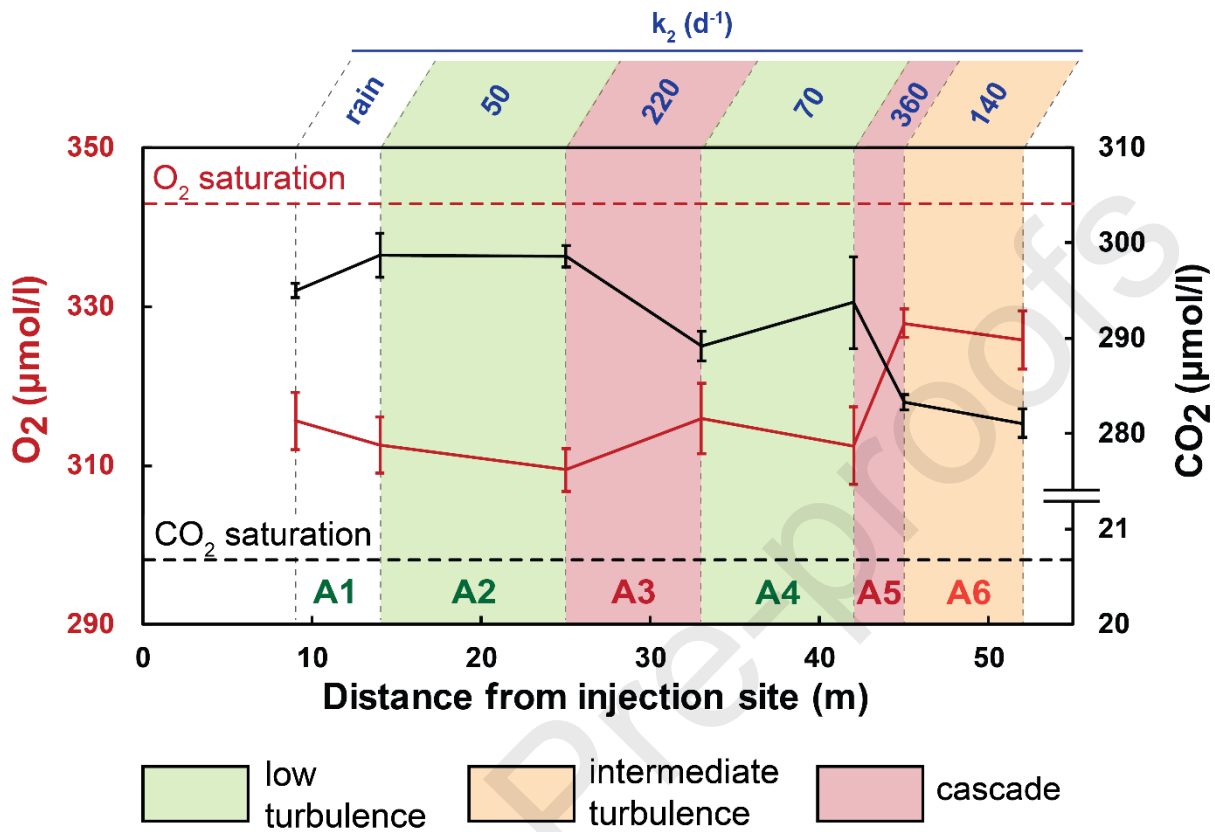

Figure 6. Cascades induce a rapid gain of O_2 (red) and release of CO2 (black) along stream A. Errors bars represent ± σ. Dashed lines indicate O_2 (red) and CO_2 (black) equilibrium with the atmosphere. k_2 values obtained by helium injection are recalled on the top of the graph and area colors indicate the visually-determined level of turbulence.

Based on the mean CO_2 concentration of stream A and the gas exchange rate coefficient measured with helium and converted to CO_2 (equation 4), we estimated the global CO_2 evasion rate of stream A at 47 µmol m^{-2} s^{-1} (equation 6). This corresponds to 48 gC m^{-2} d^{-1}, which is close to the evasion rate of 56 gC m^{-2} d^{-1} that

was measured in a Canadian steep headwater stream by direct CO_2 injections (McDowell and Johnson 2018). The CO_2 evasion rate of stream A was also calculated using the gas exchange rate coefficients predicted by the empirical equations of table 2. It yielded systematically lower CO_2 evasion rates, comprised between 16 and 44 gC m^{-2} d^{-1} (table 6). Thus, the underestimation of gas exchange rate coefficients by empirical equations (section 3.2.) leads to a significant underestimation of the CO_2 flux from headwater streams.

If CO_2 concentrations in the stream were modified solely by gas exchanges with the atmosphere, the calculated evasion rate of 48 gC m^{-2} d^{-1} would imply a decrease of 50 µmol L^{-1} in the CO_2 concentration between the upstream and the downstream end of the reach A. This is higher than the measured net loss of CO_2, close to 20 µmol L^{-1} (Figure 6), showing that other processes, such as oxygenic respiration, partly counterbalance the loss of CO_2 to the atmosphere. It highlights that the CO_2 evasion rates cannot be derived directly from the changes in CO_2 concentration along the streams.

Table 6. CO_2 evasion rate in stream A derived from the gas exchange rate coefficients obtained with the equations of table 2. Predictive equations of gas exchange rate coefficients lead to an underestimation of CO_2 evasion rate.

Gas exchange coefficient based on		CO_2 evasion rate ($gC\ m^{-2}\ d^{-1}$)
This experiment		**48**
O'Connor and Dobbins (1958)		16
Melching and Flores (1999)		24
Gualtieri and Gualtieri (2000) Gualtieri et al. (2002)		23
Raymond et al. (2012)	[1]	29
	[2]	29
	[3]	33
	[4]	33
	[5]	30
	[6]	32
	[7]	44

4. DISCUSSION

4.1. Predictions of gas exchanges

Comparison between measured and predicted k_2 values demonstrates that the presence of a few cascades along a stream significantly biases global predictions of gas exchange, leading to a systematic underestimation of reaeration rate coefficients. This is consistent with the study of Ulseth et al. (2019), showing, at stream scale,

that empirical models underestimate gas exchanges in high-channel slope streams. McDowell and Johnson (2018) also highlighted, when studying a headwater stream, that models underestimate gas exchange rate coefficients for high *k* values.

Processes governing gas exchanges in cascades fundamentally differ from those in flowing sections (section 2.5). In cascades, air bubbles have a strong control over gas exchanges (Chanson 1995; Chanson and Toombes 2002; Cirpka et al. 1993). Overlooking specific processes occurring in cascades leads to an underestimation of gas exchanges in headwater catchments, where shallow streams often display natural cascades. Increasing the reliability of predictions would require separate consideration of low-turbulent zones and cascades. For low-turbulent stream sections, our study confirms the predictive capacities of the empirical and semi-empirical equations of table 2. For cascades, predictions are more challenging and require additional morphological characterization or field experiments. Studies focused on spillways in flumes (Baylar et al. 2006; Essery et al. 1978; Gameson 1957; Gulliver et al. 1998; Khdhiri et al. 2014; Tebbutt 1972; Toombes and Chanson 2005) and on dams (Caplow et al. 2004; Gamlin et al. 2001) or cascades (Cirpka et al. 1993) in rivers, use the aeration efficiency E instead of the gas exchange rate coefficient k. Aeration efficiency was defined by Gameson (1957) and represents the total change in gas concentration occurring in the cascade, normalized by the air-water concentration gradient:

$$E = \frac{C_{down} - C_{up}}{C_{eq} - C_{up}} \tag{7}$$

where C_{up} (mol L^{-1}) is the upstream concentration, C_{down} (mol L^{-1}) is the downstream concentration and C_{eq} (mol L^{-1}) is the dissolved gas concentration at equilibrium with the atmosphere. Equations derived from lab experiments predict aeration efficiency as a function of cascade total height and, if applicable, of additional morphological parameters of the cascade such as the height of intermediate steps, or the angle of the weir (Baylar and Bagatur 2006; Baylar et al. 2006; Baylar et al. 2011; Essery et al. 1978; Khdhiri et al. 2014). The morphological characteristics of the hydraulic structure seem to be more reliable to predict aeration in cascades than the depth of the water layer. However, if these morphological characteristics are well-defined in flumes, they are much harder to describe properly in natural streams, where cascades are made up of heterogeneous stones and pieces of wood. For more accurate gas exchange quantification, direct measurements remain necessary in cascades.

4.2. Impact of cascades on groundwater discharge estimates

Groundwater discharge in streams is commonly quantified using the natural gas tracer ^{222}Rn. Some authors like Gilfedder et al. (2019) and Cartwright et al. (2014) raised the question of the impact of the variability of turbulence on ^{222}Rn degassing rate and thus on groundwater discharge estimation. Our study points out that cascades, by generating a fast equilibration between the stream and the atmosphere, erase an important part of the gaseous groundwater signal in the stream (e.g. Rn, He, Ar, CO_2, CH_4, N_2, N_2O). A cascade that is a few tens of centimeters high can lose as much gas as a hundred meter long stream. Since such cascades are very common in

low-order streams, this is prone to yield an underestimation of the groundwater discharge calculated by ^{222}Rn mass balances. The location of the cascades should be taken into account when defining the ^{222}Rn sampling strategy and their number and size between the up and down ^{222}Rn sampling locations minimized. Our results suggest that in reaches without notable cascades, one can reasonably calculate the ^{222}Rn degassing rate with empirical equations. In reaches displaying notable cascades, however, direct gas tracer experiments appear to be necessary.

4.3. Hot spots of reaeration

Studies based on flume experiments recommend the use of dams in rivers subject to eutrophication to enhance water reaeration (Tebbutt 1972). Our study shows that natural cascades significantly increase the oxygenation of headwater streams. In this way, they might strongly help sustaining aerobic metabolism, and thus provide a crucial ecosystem service in headwater catchment subject to eutrophication (Dodds and Smith 2016; Garnier and Billen 2007). Considered as reaeration hot spots, small cascades have the potential to enhance measurably the ecological conditions of eutrophic streams and might thus be considered in management and restoration strategies (Palmer et al. 2005).

4.4. Hot spots of CO_2 emission

Most headwater streams are net sources of atmospheric CO_2 (Cole et al. 2007; Marx et al. 2017). Indeed, organic matter respiration occurring in the contributing compartments (aquifer, hyporheic zone, soil) and in the stream network itself is often responsible for an oversaturation in CO_2 (Cole et al. 2007) compared to the

equilibrium with the atmosphere. Drops in CO_2 partial pressure in water after cascades and highly turbulent zones have been evidenced in headwater streams (Duvert et al. 2018; Leibowitz et al. 2017; Natchimuthu et al. 2017). In karst systems, these drops have been linked to water softening (Chen et al. 2004). At a much bigger scale, Liu et al. (2017) showed that CO_2 outgassing from low-gradient large rivers was strongly controlled by the geomorphology. Here, by simultaneously mapping the loss of a gas tracer and the changes in CO_2 concentration along a headwater stream, we establish a direct link between streambed morphology, gas exchanges, and CO_2 release to the atmosphere. We show that cascades significantly enhance gas exchanges, leading to a fast CO_2 release to the atmosphere. In a study focused on the temporal variability of gas exchanges, McDowell and Johnson (2018) showed that 84% of CO_2 emissions from a steep headwater stream occurred when discharge was higher than the median. They suggested that high flow events, because they increase turbulence, can be seen as "hot moments" of CO_2 emission in headwater streams (McClain et al. 2003). Here, we highlight the spatial variability of CO_2 emissions and show that similarly, by increasing gas exchanges, cascades can be viewed as "hot spots" of CO_2 emission in headwater streams.

If we assume the 19 km-long first order stream network of our 35 km^2 catchment has the same CO_2 emission rate as the studied stream A, a rough estimate of the total evasion of CO_2 over all first-order streams of the catchment can be calculated. We limit the upscaling to the first-order stream network of a small catchment, in which we assume that on average, cascades have the frequency and the size of those of

stream A. Predictive equations from table 2 would lead to a total CO_2 emission comprised between 150 and 300 tC year^{-1} with the mean of the outputs from the ten equations being 220 tC year^{-1}, while the measured gas exchange rate leads to a CO_2 emission of 330 tC year^{-1}. Such a rough, first-order estimation indicates that the prediction of gas exchange rate coefficients at a large-scale with empirical equations is likely to induce a general underestimation of CO_2 emission from headwater catchments. Similarly, empirical equations probably lead to an underestimation of the emission of other greenhouse gases such as CH_4.

5. CONCLUSION

Using continuous helium injection, we mapped gas exchanges along two low-slope headwater streams in a temperate catchment in Brittany (France). Our experimental set-up took advantage of the real-time data visualization allowed by the *in-situ* CF-MIMS. It highlights the new opportunities offered by this technology, in terms of spatial as well as temporal characterization of gas exchange processes. The semi-continuous measurements allow to visualize and to quantify the uncertainties.

We evidenced a high spatial variability of gas exchanges, related to the small-scale heterogeneity of the streambed morphology, which is a characteristic feature of headwater streams. During one of our tracer tests, a small cascade was responsible for almost half of the helium loss, while it occupied less than 4% of the total stream length. Nevertheless, the equations predicting the gas exchange rate coefficients in headwater streams do not account for the specific processes governing gas

exchanges in natural cascades. As a result, while empirical relationships perform well in low-turbulent zones, they systematically underestimate gas exchange rate coefficients as soon as small cascades are present. This highlights the necessity of performing direct measurements of gas exchange rate coefficients in reaches displaying cascades while low-turbulent zones can be efficiently characterized by empirical equations.

Additional CO_2 and O_2 measurements highlighted that small cascades strongly modify the chemical state of headwater streams. High gas exchange rate coefficients allow a fast incorporation of O_2 in the water and a fast release of CO_2 to the atmosphere. Thus, cascades sustain respiration by rebalancing O_2 concentrations in the stream. At the same time, they promote the evasion of the oversaturated CO_2 to the atmosphere. Finally, small natural cascades are hot spots for both stream oxygenation and greenhouse gas emission. Rough calculations of CO_2 emissions showed that the use of empirical equations leads to an underestimation of global CO_2 emissions from headwater streams. Since the small-scale morphological heterogeneity is a characteristic feature of headwater streams, the upscaling effort could be helped by a distinct consideration of cascades and low-turbulent sections. The first step would be to separately characterize gas exchange processes in these totally different hydrodynamic regimes. The second step would be to estimate the proportion of these two regimes in the stream network. This could be helped by innovative technologies such as LIDAR, allowing a fine-scale characterization of the topography.

ACKNOLEDGMENTS

PhD of Camille Vautier is funded by the French Ministry for Higher Education, Research and Innovation. Most of the equipment, especially the CF-MIMS, was funded by the CRITEX project (ANR-11-EQPX-0011). Analysis with µGC were performed within the CONDATE-EAU analytical platform in Rennes. Field work was performed in the Long-Term Socio-Ecological Research (LTSER) site "Zone Atelier Armorique". The authors thank Christophe Petton and Virginie Vergnaud for their precious involvement in the field experiments and in the laboratory analysis. We also greatly thank Madeleine Nicolas for the proof-reading of the manuscript. We thank the four reviewers, including Jordan F. Clark, for constructive comments and suggestions.

APPENDIX A: supplementary data

- Figure A.1: Photograph of the bubbling system
- Figure A.2: Entire time series of the monitoring of helium
- Table A.1: Hydraulic and morphologic characteristics of reaches A and B
- Table A.2: Test of the stability of the plateaus of helium concentration

REFERENCES

Aristegi, L., O. Izagirre & A. Elosegi, 2009. Comparison of several methods to calculate reaeration in streams, and their effects on estimation of metabolism. Hydrobiologia 635(1):113-124 doi:10.1007/s10750-009-9904-8.

Avery, E., R. Bibby, A. Visser, B. Esser & J. Moran, 2018. Quantification of Groundwater Discharge in a Subalpine Stream Using Radon-222. Water 10(2) doi:10.3390/w10020100.

Baird, M. H. I. & J. F. Davidson, 1962. Annular jets—II: Gas absorption. Chemical Engineering Science 17(6):473-480 doi:https://doi.org/10.1016/0009-2509(62)85016-7.

Baylar, A. & T. Bagatur, 2006. Experimental studies on air entrainment and oxygen content downstream of sharp-crested weirs. Water and Environment Journal 20(4):210-216 doi:10.1111/j.1747-6593.2005.00002.x.

Baylar, A., M. E. Emiroglu & T. Bagatur, 2006. An experimental investigation of aeration performance in stepped spillways. Water and Environment Journal 20(1):35-42 doi:10.1111/j.1747-6593.2005.00009.x.

Baylar, A., M. Unsal & F. Ozkan, 2011. GEP modeling of oxygen transfer efficiency prediction in aeration cascades. KSCE Journal of Civil Engineering 15(5):799-804 doi:10.1007/s12205-011-1282-x.

Benson, A., M. Zane, T. Becker, A. Visser, S. Uriostegui, E. DeRubeis, J. Moran, B. Esser & J. Clark, 2014. Quantifying Reaeration Rates in Alpine Streams Using Deliberate Gas Tracer Experiments. Water 6(4):1013-1027 doi:10.3390/w6041013.

Bernot, M. J., D. J. Sobota, R. O. Hall Jr, P. J. Mulholland, W. K. Dodds, J. R. Webster, J. L. Tank, L. R. Ashkenas, L. W. Cooper, C. N. Dahm, S. V. Gregory, N. B. Grimm, S. K. Hamilton, S. L. Johnson, W. H. Mcdowell, J. L. Meyer, B. Peterson, G. C. Poole, H. M. Valett, C. Arango, J. J. Beaulieu, A. J. Burgin, C. Crenshaw, A. M. Helton, L. Johnson, J. Merriam, B. R. Niederlehner, J. M. O'brien, J. D. Potter, R. W. Sheibley, S. M. Thomas & K. Wilson, 2010. Inter-regional comparison of land-use effects on stream metabolism. Freshwater Biology 55(9):1874-1890 doi:doi:10.1111/j.1365-2427.2010.02422.x.

Billett, M. F., S. M. Palmer, D. Hope, C. Deacon, R. Storeton-West, K. J. Hargreaves, C. Flechard & D. Fowler, 2004. Linking land-atmosphere-stream carbon fluxes in a lowland peatland system. Global Biogeochemical Cycles 18(1) doi:10.1029/2003gb002058.

Bishop, K., I. Buffam, M. Erlandsson, J. Fölster, H. Laudon, J. Seibert & J. Temnerud, 2008. Aqua Incognita: the unknown headwaters. Hydrological Processes 22(8):1239-1242 doi:10.1002/hyp.7049.

Bott, T. L., D. S. Montgomery, J. D. Newbold, D. B. Arscott, C. L. Dow, A. K. Aufdenkampe, J. K. Jackson & L. A. Kaplan, 2006. Ecosystem metabolism in streams of the Catskill Mountains (Delaware and Hudson River watersheds) and Lower Hudson Valley. J N Am Benthol Soc 25(4):1018-1044 doi:10.1899/0887-3593(2006)025[1018:Emisot]2.0.Co;2.

Caplow, T., P. Schlosser & T. Ho David, 2004. Tracer Study of Mixing and Transport in the Upper Hudson River with Multiple Dams. Journal of Environmental Engineering 130(12):1498-1506 doi:10.1061/(ASCE)0733-9372(2004)130:12(1498).

Carlson, T., 1911. The diffusion of oxygen in water. Journal of the American Chemical Society 33(7):1027-1032 doi:10.1021/ja02220a002.

Cartwright, I., H. Hofmann, B. Gilfedder & B. Smyth, 2014. Understanding parafluvial exchange and degassing to better quantify groundwater inflows using 222Rn: The King River, southeast Australia. Chemical Geology 380:48-60 doi:10.1016/j.chemgeo.2014.04.009.

Chanson, H., 1995. Air-water gas transfer at hydraulic jump with partially developed inflow. Water Research 29(10):2247-2254 doi:https://doi.org/10.1016/0043-1354(95)00056-Q.

Chanson, H. & L. Toombes, 2002. Air–water flows down stepped chutes: turbulence and flow structure observations. International Journal of Multiphase Flow 28(11):1737-1761 doi:https://doi.org/10.1016/S0301-9322(02)00089-7.

Chatton, E., T. Labasque, J. de La Bernardie, N. Guiheneuf, O. Bour & L. Aquilina, 2017. Field Continuous Measurement of Dissolved Gases with a CF-MIMS: Applications to the Physics and Biogeochemistry of Groundwater Flow. Environ Sci Technol 51(2):846-854 doi:10.1021/acs.est.6b03706.

Chen, J., D. D. Zhang, S. J. Wang & T. F. Xiao, 2004. Water self-softening processes at waterfall sites. Acta Geol Sin-Engl Ed 78(5):1154-1161.

Churchill, M. A., H. L. Elmore & R. A. Buckingham, 1964. The prediction of stream reaeration rates. In Southgate, B. A. (ed) Advances in Water Pollution Research. Pergamon, 89-136.

Cirpka, O., P. Reichert, O. Wanner, S. R. Mueller & R. P. Schwarzenbach, 1993. Gas exchange at river cascades: field experiments and model calculations. Environ Sci Technol 27(10):2086-2097 doi:10.1021/es00047a014.

Cole, J. J., Y. T. Prairie, N. F. Caraco, W. H. McDowell, L. J. Tranvik, R. G. Striegl, C. M. Duarte, P. Kortelainen, J. A. Downing, J. J. Middelburg & J. Melack, 2007. Plumbing the Global Carbon Cycle: Integrating Inland Waters into the Terrestrial Carbon Budget. Ecosystems 10(1):172-185 doi:10.1007/s10021-006-9013-8.

Cook, P. G., G. Favreau, J. C. Dighton & S. Tickell, 2003. Determining natural groundwater influx to a tropical river using radon, chlorofluorocarbons and ionic environmental tracers. Journal of Hydrology 277(1-2):74-88 doi:10.1016/s0022-1694(03)00087-8.

Crawford, J. T., N. R. Lottig, E. H. Stanley, J. F. Walker, P. C. Hanson, J. C. Finlay & R. G. Striegl, 2014. CO2and CH4emissions from streams in a lake-rich landscape: Patterns, controls, and regional significance. Global Biogeochemical Cycles 28(3):197-210 doi:10.1002/2013gb004661.

Dodds, W. & V. Smith, 2016. Nitrogen, phosphorus, and eutrophication in streams. Inland Waters 6(2):155-164 doi:10.5268/iw-6.2.909.

Duvert, C., D. E. Butman, A. Marx, O. Ribolzi & L. B. Hutley, 2018. CO2 evasion along streams driven by groundwater inputs and geomorphic controls. Nature Geoscience 11(11):813-818 doi:10.1038/s41561-018-0245-y.

Essery, I. T. S., T. H. Y. Tebbutt & S. K. Rajaratnam, 1978. Design of Spillways for Reaeration of Polluted Waters. CIRIA Report No 72, Jan London, UK:36.

Gameson, A. L. H., 1957. Weirs and aeration of rivers. J Inst Water Eng 11:477-490.

Gamlin, J. D., J. F. Clark, G. Woodside & R. Herndon, 2001. Large-Scale Tracing of Ground Water with Sulfur Hexafluoride. Journal of Environmental Engineering 127(2):171-174 doi:doi:10.1061/(ASCE)0733-9372(2001)127:2(171).

Garnier, J. & G. Billen, 2007. Production vs. respiration in river systems: an indicator of an "ecological status". The Science of the total environment 375(1-3):110-24 doi:10.1016/j.scitotenv.2006.12.006.

Genereux, D. P. & H. F. Hemond, 1990. Naturally Occurring Radon 222 as a Tracer for Streamflow Generation: Steady State Methodology and Field Example. Water Resources Research 26(12):3065-3075 doi:doi:10.1029/WR026i012p03065.

Genereux, D. P. & H. F. Hemond, 1992. Determination of gas exchange rate constants for a small stream on Walker Branch Watershed, Tennessee. Water Resources Research 28(9):2365-2374 doi:doi:10.1029/92WR01083.

Gilfedder, B. S., I. Cartwright, H. Hofmann & S. Frei, 2019. Explicit Modeling of Radon-222 in HydroGeoSphere During Steady State and Dynamic Transient Storage. Groundwater 57(1):36-47 doi:10.1111/gwat.12847.

Gleeson, T., A. H. Manning, A. Popp, M. Zane & J. F. Clark, 2018. The suitability of using dissolved gases to determine groundwater discharge to high gradient streams. Journal of Hydrology 557:561-572 doi:10.1016/j.jhydrol.2017.12.022.

Goncalves, J., A. Silveira, G. B. Lopes, M. S. da Luz & A. L. A. Simoes, 2017. Reaeration Coefficient Estimate: New Parameter for Predictive Equations. Water Air Soil Pollut 228(8):10 doi:10.1007/s11270-017-3491-5.

Gualtieri, C. & P. Gualtieri, 2000. Field verification for a reaeration model in streams. Paper presented at the 4th International Conference On Hydroscience & Engineering, Seoul, Korea.

Gualtieri, C., P. Gualtieri & G. P. Doria, 2002. Dimensional analysis of reaeration rate in streams. Journal of Environmental Engineering-Asce 128(1):12-18 doi:10.1061/(asce)0733-9372(2002)128:1(12).

Gulliver, J., S., S. Wilhelms, C. & K. Parkhill, L., 1998. Predictive Capabilities in Oxygen Transfer at Hydraulic Structures. Journal of Hydraulic Engineering 124(7):664-671 doi:10.1061/(ASCE)0733-9429(1998)124:7(664).

Haider, H., W. Ali & S. Haydar, 2013. Evaluation of various relationships of reaeration rate coefficient for modeling dissolved oxygen in a river with extreme flow variations in Pakistan. Hydrological Processes 27(26):3949-3963 doi:10.1002/hyp.9528.

Hall, R. O. & H. L. Madinger, 2018. Use of argon to measure gas exchange in turbulent mountain streams. Biogeosciences 15(9):3085-3092 doi:10.5194/bg-15-3085-2018.

Ho, D. T., W. E. Asher, L. F. Bliven, P. Schlosser & E. L. Gordan, 2000. On mechanisms of rain-induced air-water gas exchange. Journal of Geophysical Research: Oceans 105(C10):24045-24057 doi:10.1029/1999jc000280.

Hope, D., S. M. Palmer, M. F. Billett & J. J. C. Dawson, 2001. Carbon dioxide and methane evasion from a temperate peatland stream. Limnology and Oceanography 46(4):847-857 doi:doi:10.4319/lo.2001.46.4.0847.

Jähne, B., G. Heinz & W. Dietrich, 1987a. Measurement of the diffusion coefficients of sparingly soluble gases in water. Journal of Geophysical Research 92(C10):10767 doi:10.1029/JC092iC10p10767.

Jähne, B., K. O. Münnich, R. Bösinger, A. Dutzi, W. Huber & P. Libner, 1987b. On the parameters influencing air-water gas exchange. Journal of Geophysical Research: Oceans 92(C2):1937-1949 doi:doi:10.1029/JC092iC02p01937.

Khdhiri, H., O. Potier & J. P. Leclerc, 2014. Aeration efficiency over stepped cascades: better predictions from flow regimes. Water Res 55:194-202 doi:10.1016/j.watres.2014.02.022.

Kilpatrick, F. A., R. E. Rathbun, N. Yotsukura, G. W. Parker & L. L. DeLong, 1987. Determination of stream reaeration coefficients by use of tracers Open-File Report.

Knapp, J. L., K. Osenbruck & O. A. Cirpka, 2015. Impact of non-idealities in gas-tracer tests on the estimation of reaeration, respiration, and photosynthesis rates in streams. Water Res 83:205-16 doi:10.1016/j.watres.2015.06.032.

Knapp, J. L. A., K. Osenbrück, M. S. Brennwald & O. A. Cirpka, 2019. In-situ mass spectrometry improves the estimation of stream reaeration from gas-tracer tests. Science of The Total Environment 655:1062-1070 doi:https://doi.org/10.1016/j.scitotenv.2018.11.300.

Kolbe, T., J. Marcais, Z. Thomas, B. W. Abbott, J. R. de Dreuzy, P. Rousseau-Gueutin, L. Aquilina, T. Labasque & G. Pinay, 2016. Coupling 3D groundwater modeling with CFC-based age dating to classify local groundwater circulation in an unconfined crystalline aquifer. Journal of Hydrology 543:31-46 doi:10.1016/j.jhydrol.2016.05.020.

Lauerwald, R., G. G. Laruelle, J. Hartmann, P. Ciais & P. A. G. Regnier, 2015. Spatial patterns in CO_2 evasion from the global river network. Global Biogeochemical Cycles 29(5):534-554 doi:10.1002/2014gb004941.

Leibowitz, Z. W., L. A. F. Brito, P. V. De Lima, E. M. Eskinazi-Sant'Anna & N. O. Barros, 2017. Significant changes in water pCO_2 caused by turbulence from waterfalls. Limnologica 62:1-4 doi:10.1016/j.limno.2016.09.008.

Liu, S., X. X. Lu, X. Xia, X. Yang & L. Ran, 2017. Hydrological and geomorphological control on CO2 outgassing from low-gradient large rivers: An example of the Yangtze River system. Journal of Hydrology 550:26-41 doi:10.1016/j.jhydrol.2017.04.044.

Marx, A., J. Dusek, J. Jankovec, M. Sanda, T. Vogel, R. van Geldern, J. Hartmann & J. A. C. Barth, 2017. A review of CO2 and associated carbon dynamics in headwater streams: A global perspective. Rev Geophys 55(2):560-585 doi:10.1002/2016rg000547.

McClain, M. E., E. W. Boyer, C. L. Dent, S. E. Gergel, N. B. Grimm, P. M. Groffman, S. C. Hart, J. W. Harvey, C. A. Johnston, E. Mayorga, W. H. McDowell & G. Pinay, 2003. Biogeochemical Hot Spots and Hot Moments at the Interface of Terrestrial and Aquatic Ecosystems. Ecosystems 6(4):301-312 doi:10.1007/s10021-003-0161-9.

McDowell, M. J. & M. S. Johnson, 2018. Gas Transfer Velocities Evaluated Using Carbon Dioxide as a Tracer Show High Streamflow to Be a Major Driver of Total CO2 Evasion Flux for a Headwater Stream. Journal of Geophysical Research: Biogeosciences 123(7):2183-2197 doi:10.1029/2018jg004388.

Melching, C. S. & H. E. Flores, 1999. Reaeration equations derived from US geological survey database. Journal of Environmental Engineering-Asce 125(5):407-414 doi:10.1061/(asce)0733-9372(1999)125:5(407).

Mulholland, P. J., C. S. Fellows, J. L. Tank, N. B. Grimm, J. R. Webster, S. K. Hamilton, E. Martí, L. Ashkenas, W. B. Bowden, W. K. Dodds, W. H. Mcdowell, M. J. Paul & B. J. Peterson, 2001. Inter-biome comparison of factors controlling stream metabolism. Freshwater Biology 46(11):1503-1517 doi:doi:10.1046/j.1365-2427.2001.00773.x.

Natchimuthu, S., M. B. Wallin, L. Klemedtsson & D. Bastviken, 2017. Spatio-temporal patterns of stream methane and carbon dioxide emissions in a hemiboreal catchment in Southwest Sweden. Sci Rep 7:39729 doi:10.1038/srep39729.

O'Connor, D. J. & W. E. Dobbins, 1958. Mechanism of Reaeration in Natural Streams. Transactions of the American Society of Civil Engineers 123(1):641-666.

Öquist, M. G., M. Wallin, J. Seibert, K. Bishop & H. Laudon, 2009. Dissolved Inorganic Carbon Export Across the Soil/Stream Interface and Its Fate in a Boreal Headwater Stream. Environ Sci Technol 43(19):7364-7369 doi:10.1021/es900416h.

Palmer, M. A., E. S. Bernhardt, J. D. Allan, P. S. Lake, G. Alexander, S. Brooks, J. Carr, S. Clayton, C. N. Dahm, J. Follstad Shah, D. L. Galat, S. G. Loss, P. Goodwin, D. D. Hart, B. Hassett, R. Jenkinson, G. M. Kondolf, R. Lave, J. L. Meyer, T. K. O'Donnell, L. Pagano & E. Sudduth, 2005. Standards for

ecologically successful river restoration. Journal of Applied Ecology 42(2):208-217 doi:10.1111/j.1365-2664.2005.01004.x.

Palumbo, J. E. & L. C. Brown, 2014. Assessing the Performance of Reaeration Prediction Equations. Journal of Environmental Engineering 140(3):7 doi:10.1061/(asce)ee.1943-7870.0000799.

Raymond, P. A., C. J. Zappa, D. Butman, T. L. Bott, J. Potter, P. Mulholland, A. E. Laursen, W. H. McDowell & D. Newbold, 2012. Scaling the gas transfer velocity and hydraulic geometry in streams and small rivers. Limnology and Oceanography: Fluids and Environments 2(1):41-53 doi:10.1215/21573689-1597669.

Riley, A. J. & W. K. Dodds, 2012. Whole-stream metabolism: strategies for measuring and modeling diel trends of dissolved oxygen. Freshwater Science 32(1):56-69, 14.

Ritz, S., K. Dähnke & H. Fischer, 2017. Open-channel measurement of denitrification in a large lowland river. Aquatic Sciences 80(1) doi:10.1007/s00027-017-0560-1.

Soares, P. A., G. Faht, A. Pinheiro, M. R. da Silva & E. Zucco, 2013. Determination of reaeration-rate coefficient by modified tracer gas technique. Hydrological Processes 27(19):2710-2720 doi:10.1002/hyp.9371.

Tebbutt, T. H. Y., 1972. Some studies on reaeration in cascades. Water Research 6(3):297-304 doi:https://doi.org/10.1016/0043-1354(72)90007-3.

Tobias, C. R., J. K. Bohlke, J. W. Harvey & E. Busenberg, 2009. A simple technique for continuous measurement of time-variable gas transfer in surface waters. Limnol Oceanogr Meth 7:185-195 doi:10.4319/lom.2009.7.185.

Toombes, L. & H. Chanson, 2005. Air-Water Mass Transfer on a Stepped Waterway. Journal of Environmental Engineering 131(10):1377-1386 doi:doi:10.1061/(ASCE)0733-9372(2005)131:10(1377).

Tranvik, L. J., J. A. Downing, J. B. Cotner, S. A. Loiselle, R. G. Striegl, T. J. Ballatore, P. Dillon, K. Finlay, K. Fortino, L. B. Knoll, P. L. Kortelainen, T. Kutser, S. Larsen, I. Laurion, D. M. Leech, S. L. McCallister, D. M. McKnight, J. M. Melack, E. Overholt, J. A. Porter, Y. Prairie, W. H. Renwick, F. Roland, B. S. Sherman, D. W. Schindler, S. Sobek, A. Tremblay, M. J. Vanni, A. M. Verschoor, E. von Wachenfeldt & G. A. Weyhenmeyer, 2009. Lakes and reservoirs as regulators of carbon cycling and climate. Limnology and Oceanography 54(6, part 2):2298-2314 doi:doi:10.4319/lo.2009.54.6_part_2.2298.

Tsivoglou, E. C. & L. A. Neal, 1976. Tracer Measurement of Reaeration: III. Predicting the Reaeration Capacity of Inland Streams. Journal (Water Pollution Control Federation) 48(12):2669-2689.

Ulseth, A. J., R. O. Hall, M. Boix Canadell, H. L. Madinger, A. Niayifar & T. J. Battin, 2019. Distinct air–water gas exchange regimes in low- and high-energy streams. Nature Geoscience 12(4):259-263 doi:10.1038/s41561-019-0324-8.

Wallin, M. B., M. G. Öquist, I. Buffam, M. F. Billett, J. Nisell & K. H. Bishop, 2011. Spatiotemporal variability of the gas transfer coefficient (KCO2) in boreal streams: Implications for large scale estimates of CO2evasion. Global Biogeochemical Cycles 25(3) doi:10.1029/2010gb003975.

Wanninkhof, R., 1992. Relationship between wind speed and gas exchange over the ocean. Journal of Geophysical Research 97(C5):7373 doi:10.1029/92jc00188.

Wanninkhof, R., P. J. Mulholland & J. W. Elwood, 1990. Gas exchange rates for a first-order stream determined with deliberate and natural tracers. Water Resources Research 26(7):1621-1630 doi:doi:10.1029/WR026i007p01621.

Weber, U. W., P. G. Cook, M. S. Brennwald, R. Kipfer & T. C. Stieglitz, 2019. A Novel Approach To Quantify Air-Water Gas Exchange in Shallow Surface Waters Using High-Resolution Time Series of Dissolved Atmospheric Gases. Environ Sci Technol 53(3):1463-1470 doi:10.1021/acs.est.8b05318.

Wise, D. L. & G. Houghton, 1966. The diffusion coefficients of ten slightly soluble gases in water at 10–60°C. Chemical Engineering Science 21(11):999-1010 doi:https://doi.org/10.1016/0009-2509(66)85096-0.

Young, R. G. & A. D. Huryn, 1998. Comment: Improvements to the diurnal upstream-downstream dissolved oxygen change technique for determining whole-stream metabolism in small streams. Canadian Journal of Fisheries and Aquatic Sciences 55(7):1784-1785 doi:10.1139/f98-052.

Young, R. G. & A. D. Huryn, 1999. Effects of land use on stream metabolism and organic matter turnover. Ecological Applications 9(4):1359-1376 doi:10.1890/1051-0761(1999)009[1359:Eoluos]2.0.Co;2.

Camille Vautier: Conceptualization, Methodology, Investigation, Visualization, Writing - Original Draft. **Ronan Abhervé:** Conceptualization, Methodology, Investigation, Visualization. **Thierry Labasque:** Conceptualization, Methodology, Investigation. **Anniet M. Laverman:** Writing - Review & Editing. **Aurélie Guillou:** Investigation. **Eliot Chatton:** Methodology, Investigation. **Pascal Dupont:** Conceptualization. **Luc Aquilina:** Conceptualization, Writing - Review & Editing. **Jean-Raynald de Dreuzy:** Conceptualization, Writing - Review & Editing, Supervision.

Declaration of interests

☒ The authors declare that they have no known competing financial interests or personal relationships that could have appeared to influence the work reported in this paper.

☐The authors declare the following financial interests/personal relationships which may be considered as potential competing interests: